JMEPEG (1996) 5:489-499

Application of the Finite-Element Method to a Design of Optimized Tool Geometry for the O.S.U. Formability Test

Y.S. Suh and R.H. Wagoner

A new, plane-strain, sheet-formability test (the O.S.U. Formability Test, OSUFT) has been recently proposed, and it has shown many improvements over the limiting dome height (LDH) test. However, the prototype tool geometry was initially determined arbitrarily for the experiment so that an enhancement of the tool geometry was made with dual purpose: to design the tool geometry to generate consistent plane-strain state up to failure under various lubrication states and different testing materials and, at the same time, to make the testing equipment cost as low as possible so that the test may be readily available for small- and medium-scale stamping companies. The latter demands a compact tool geometry to minimize the required press capacity, while the former requires wider blanks that increase the punch load. Considering these conflicting conditions, computer simulation technique using three-dimensional finite-element method was introduced, rather than performing numerous die tryouts, to design the optimal tool geometry from simulative trial and error. By reducing the size of the entire tool and controlling the width-to-length ratio of the blank, an enhanced tool geometry was found that generates stable plane-strain state up to failure and still features low required load capacity for materials with *r*-values up to 2.0, friction coefficient ranges of 0.15 to approximately 0.35, and thicknesses up to 1.5 mm. The bending-dominant failure due to smaller radii of the tool was avoided. Comparison of LDH simulation showed that the enhanced configuration of the test will produce more proportional strain path and larger plane-strain area near the predicted failure region. It was also predicted that the testing results will be less sensitive to the lubrication state on the tool surface and the material anisotropy of the sheet, which will contribute to a better repeatability of the test. Experiments revealed that the optimized tool showed significantly less scatter in measurement compared with that of the LDH and the original O.S.U. formability tests.

Keywords

finite-element method, optimized tool geometry, sheet-formability test, O.S.U. formability test

1. Introduction

A FAST and accurate sheet-formability test is desirable for use in stamping plants and by the distributors and suppliers of sheet product. At present, no universal test is available to evaluate sheet formability for various stamping processes. While several kinds of simulative formability tests such as Swift, Olsen, Erichsen, and Fukui cup tests have been used in the past (Ref 1, 2), only the limiting dome height test (LDH) (Ref 3, 4) has been the subject of recent widespread qualification (Ref 5-7). The LDH test simulates stretching processes using a spherical punch and a rectangular blank with optimal blank width that generates the best plane-strain state near the failure region. In general, more than 85% of split-type failures in stable stamping line take place at or near the plane-strain condition so that the stretching formability at plane-strain state is invaluable for assessing the general stamping formability of the sheet.

The LDH test, however, is inconvenient and expensive for routine use because of the multiple tests required for each material, the high capital cost for equipment to perform the test, and the high facility-to-facility scatter observed (Ref 8). To improve in these areas, a new plane-strain sheet formability test (or the O.S.U. Formability Test, OSUFT) makes use of generally cylindrical geometry to provide stable plane-strain states without multiple pretests of various blank widths. The new test exhibits large improvements in speed and accuracy (Ref 8, 9). Nevertheless, because the prototype tooling of the test was arbitrarily determined for the experiment, two design enhancements of the tool geometry were sought. First, the test should accommodate a stable plane strain up to failure on the blank for relatively wider ranges of lubrication states and sheet materials. This requires the use of wider blank width (i.e., wider punch width) to have less minor strain in the lateral direction (perpendicular to the stretching direction). This in turn would result in a higher punch force at failure and thus demand a larger load capacity of the press. The second enhancement was the reduction of the total equipment cost. The major obstacle to wide acceptance of a formability test for material qualification by sheet users and suppliers lies in the equipment cost. In order to provide small- and medium-sized sheet-forming companies with a low-cost formability system based on the OSUFT, the tooling had to be as compact as possible to reduce the press capacity, which is a major factor in the total equipment cost. A simple reduction of scale, however, may degenerate the plane-strain state on the blank and may lead to unwanted bending-dominant failure at the tight tool radii. Therefore, a project was initiated aiming at reducing the load capacity of the test while extending its application to wider ranges of process conditions such as lubrication states and blank materials, maintaining the desirable features of plane-strain failure away from tool contact and insensitivity to perturbations that introduce scatter and irreproducibility. To design an optimal tool geometry from the aforementioned conflicting objectives, a simulative trial-and-error technique, using a three-dimensional finite-element

Y.S. Suh, Senior Research Scientist, Division of Systems Application, Systems Research Engineering Institute, Taejon, Korea; and **R.H. Wagoner,** Professor and Chairman, Department of Materials Science and Engineering, The Ohio State University, Columbus, Ohio.

method, was introduced. Traditional die try-out would require tremendous efforts in time and expense to do this job.

Because geometric parameters, friction coefficient, and material anisotropy interactively influence the plane-strain condition near the predicted failure region of the blank, these factors were effectively considered in two three-dimensional finite-element codes—SHEET-3, a rigid, viscoplastic finite-element code developed by Ohio State University (Columbus, OH) (Ref 10-12), and ABAQUS, a commercial, multipurpose finite-element method package (Ref 13). The former is a membrane code and was used mainly to search for optimal tool and blank geometries by taking account of material anisotropy, while the latter with continuum elements was used to examine the bending influence of the compact tool. After finding the optimal geometry that matches with design goals, the prototype modular system was made for a refinement of the design.

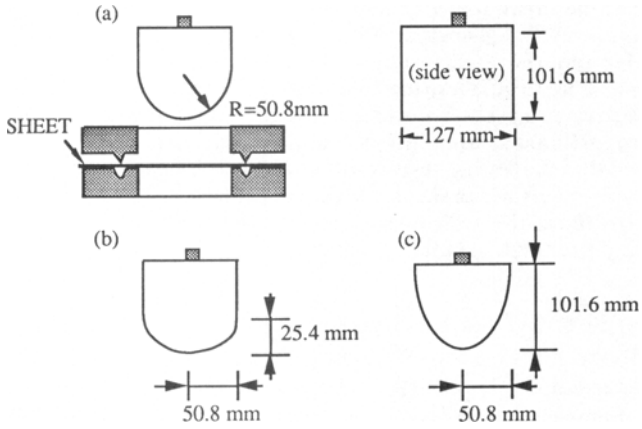

Fig. 1 Original punch geometry for OSUFT. (a) Cylindrical punch (showing both front and side views). (b) Flat-elliptical geometry. (c) Sharp-elliptical geometry

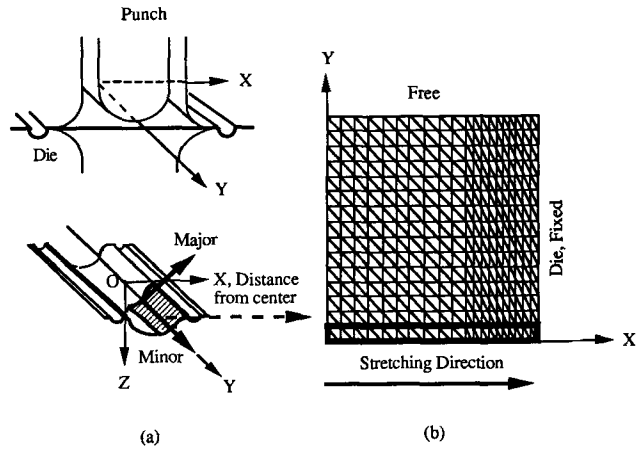

Fig. 2 Finite-element modeling of OSUFT. (a) Undeformed (above) and deformed (below) blanks with the designated direction. Major and minor directions are embedded with the blank, such that they rotate together with the material. (b) Typical finite-element meshes used with SHEET-3. For ABAQUS, similar arrangements were made with eight-node brick elements. Only one quadrant of the blank was discretized, for symmetry. The center-row elements surrounded with the bold square is the region of interest.

2. Finite-Element Modeling

At the early stage of the development of OSUFT, cylindrical, flat-elliptical, and sharp-elliptical punches were proposed (see Fig. 1). Experimentally (Ref 8, 9), the flat-elliptical punch was found to most closely exhibit plane-stain behavior and was selected in the initial modeling for the larger tooling size. Later, the cylindrical punch was chosen for the optimized compact geometry because it would generate almost the same plane-strain state as that of the flat-elliptical punch when the width-to-length aspect ratio of the blank was sufficiently large. The cylindrical geometry would provide easier manufacturing and less bending influence in comparison with the flat-elliptical geometry. The sharp-elliptical punch was not included in the analysis because its high curvature was expected to cause a large bending influence when all the dimensions were reduced. The aspect ratio of the unsupported region makes plane strain difficult to achieve in this case.

For the present analysis, SHEET-3 and ABAQUS were effectively utilized together. In SHEET-3, triangular, plane-stress membrane elements were employed. The effective stress, $\bar{\sigma}$, can be expressed using Hill's 1979 nonquadratic theory (Ref 14) in terms of principal stresses with a plane-stress assumption as follows:

$$|\sigma_1 + \sigma_2|^M + (1 + 2r)|\sigma_1 - \sigma_2|^M = 2(1 + r)\bar{\sigma}^M \qquad \text{(Eq 1)}$$

where r is the normal anisotropy parameter and M is a parameter that characterizes the shape of the yield surface. Normal anisotropy is inherent to Hill's 1979 theory with plane-stress assumption. Substituting $M = 2$ recovers the Hill's 1948 quadratic anisotropic yield function (Ref 15) and setting $r = 1$ also gives rise to the von Mises isotropic yield function. The r value can be determined from standard tensile tests, but calculation of the exponent M requires complicated testing procedures (Ref 16). A more in-depth description of SHEET-3 can be found in Ref 10 to 12. Although the membrane approximation does not account for bending, it was reported that the computation is still accurate when the ratio of the radius of curvature to the blank thickness is greater than 6 (Ref 17). Therefore, only thin blanks were involved in the SHEET-3 calculation. However, for the reduced tool size and thicker blanks, ABAQUS with solid elements were used in order to avoid bending-dominant failure due to tight radii of the compact tool. The first-order, eight-node brick, fully reduced integration elements with hourglass control (C3D8RH) were used to cope with the overconstraint from plastic incompressibility and the shear locking caused by excessive bending. While SHEET-3 provided the result associated with anisotropy, the ABAQUS computation was made with an assumption of material isotropy. The ABAQUS computation provided the 1948 Hill's anisotropic yield theory (Ref 15), with which the normal anisotropy is not easily controlled. Moreover, the 1979 Hill's yield theory implemented in the SHEET-3 could not be used even with UMAT (user subroutine) of ABAQUS because the plane-stress assumption of the

theory required use of shell element to consider bending property. At the time this work was being carried out, the ABAQUS 4.9 version did not provide appropriate finite-shell elements for the simulation of sheet-metal forming.

The meshes used for the SHEET-3 simulation were determined such that the numerical results exhibit a good agreement with the experimental data included in Ref 8. Figure 2 shows the modeling of the OSUFT and a typical mesh arrangement used with SHEET-3. Because of symmetry, only one quadrant of the blank was modeled. Finer meshes were arranged toward the die. The size and the number of the elements are varied for different sizes of test configuration. Similar arrangements were made with eight-node brick elements for ABAQUS. To improve the accuracy against the excessive stiffness of the linear brick element, smaller-sized elements were used with the ABAQUS simulation. The major (in-plane longitudinal) and minor (in-plane transverse) strains were monitored at the first row of elements along the symmetry axis of width in the stretching direction because the initiation of the failure is usually predicted in this region (see Fig. 2b). The effective stress-strain relation used in the code was of the form

$$\bar{\sigma} = K\bar{\varepsilon}^n \qquad \text{(Eq 2)}$$

with strain-hardening exponent, $n = 0.14$, and the strength coefficient, $K = 574$ MPa. This selection was examined later, and it was found that the plane-strain state did not vary much with the change of n-value. The r-value and the friction coefficient were varied to simulate different materials and lubrication conditions. The variation of the rate effect was not considered. Computations were carried out with CRAY Y-MP8/864 at the Ohio Supercomputer center.

3. Approach of Analysis

There are many parameters that can affect the plane-strain condition near the predicted failure region, but only three aspects were found to be most influential. They are:

- *The width of the blank:* A plane strain is readily predicted with wider blanks, which lead to less minor strains.
- *The normal anisotropy (r-value) of the blank material:* A higher r-value leads to a greater minor strain, and thus plane-strain state is predicted to be less likely. This was also observed experimentally (Ref 8, 9).
- *The lubrication state of the tool:* With a well-lubricated punch, the lateral material flow-in due to the diffuse neck is more allowable over the punch and the transverse strain (the minor strain in the present analysis) will be greater.

A range of friction coefficients (μ) of 0.15 to 0.35 were selected in the simulation, corresponding to a range encompassing well-lubricated condition in application up to apparently dry conditions (Ref 18). The gap between the punch and the die also affects the plane-strain condition. Like the plane-strain specimen shown in Ref 19, a lower aspect ratio of longitudinal (axial) to transverse length leads to a better plane-strain condition at the center region. In the same analogy, a smaller gap requires a shorter longitudinal length of the blank and thus leads to plane strain. However, because the gap size has a minimum limitation (where ironing occurs), a fixed value of 2.0 mm was used for the analysis except for the simulation of heavy gages thicker than 2 mm, in which case a 3.0 mm gap size was used.

The first phase of this work was focused on finding optimal blank width, which allows a stable plane-strain state near the predicted failure site and yet features a compact size that does not require increased punch force. The major strain and strain ratio monitored just before the localization at the center of the blank were evaluated for a number of different blank widths and r-values. The gap between the punch and the die (2.0 mm), the thickness of the blank (0.866 mm), the radius of the die (6.35 mm) were fixed. The sizes of the blank and the punch were varied until the final geometries were determined. To determine the optimal blank and punch geometry, a combination of parameters that would degenerate the plane-strain state near the failure site was used. The optimal size was found by constraining the ratio of major to minor strain at the predicted failure site to be greater than 5 (Ref 19).

The next phase was involved mainly in the investigation of the effect of bending with a small tool size. This test was performed using ABAQUS. The peak strains were compared to see if bending around the tighter radius influenced the failure region. The rationale of this phase was to have the predicted failure site as far as possible from the die side to avoid bending-dominant failure. A stretching-dominant failure is usually predicted by having the failure occur near the boundary of the punch-contact region or unsupported region close to it, depending on the lubrication state.

Next, two kinds of simple, numerical verifications were performed. By simulating and comparing the OSUFT with the LDH test, the performance of the optimized tool was demonstrated. Sensitivity of n, μ, r on the optimized tool was also examined. In the final phase, a prototype of tooling using the final geometry was subjected to tests for final adjustments.

4. Results and Discussion

4.1 *Phase I: Finding Optimized Tool and Blank Sizes with SHEET-3*

The first phase involved designing the OSUFT to produce plane-strain failure for a large selection of materials under a wide range of lubricating conditions with minimum punch force required. In order to achieve this, constant material and process parameters that would degenerate the plane-strain state near the predicted failure site were used. Because the less lubricated surface and lower r-value would promote the plane-strain condition as stated previously, the final tool and blank geometries that would provide a good plane-strain state were sought (the major strain should be at least five times larger than the minor strain near the predicted failure region) for a highly lubricated condition ($\mu = 0.15$, simulations of most lubricated deep-drawing operations use friction coefficients greater than this [Ref 18]) and a high r-value ($r = 2.0$, representative of the high normal anisotropy for sheet metals in general use [Ref 20]). Saunders and Wagoner (Ref 16) showed from their finite-element modeling of the OSUFT that the prediction with lower

stress exponent (M) of Hill's nonquadratic yield theory would underestimate the plane-strain condition of the OSUFT. Therefore, low M (2.0) was used in addition to aforementioned degenerating constants in order to have a conservative evaluation. If the simulative test provided the final geometry under this degenerative condition, it should ensure consistent plane-strain failure in the actual test for relatively wide range of process conditions. To measure the plane-strain condition, the peak major strain just before the localization was picked up and divided by the corresponding minor strain. The larger this ratio is, the better plane strain is represented. See Fig. 3(a) and (b).

At first, the simulation was performed with the same punch size (flat-elliptical) as the one originally proposed (see Fig. 1b), and the blank width was increased to be approximately 1.4 times larger. The results showed that the strain state at the predicted failure site was far from plane strain. In Fig. 4, even with peak major strain of 0.5, the strain localization did not take place. Figure 5 shows that most of the ratios of major to minor strain in the center along the stretch direction were less than 2. From this result it was inferred that a blank *much wider* than the one proposed was needed to get a plane-strain state for the given condition. However, such a large blank would require a large punch force and thus a large capacity of the press. Therefore, further work was focused on reducing the tool and blank sizes.

After some simulative trial and error, the punch size was reduced to one-fourth (radius = 12.7 mm) that of the size originally proposed (Ref 21). For larger ratio of blank widths to length in the stretching direction, the plane-strain state at the predicted failure site from the flat-elliptical punch was found to be similar to that from the cylindrical punch. Therefore, the cylindrical punch was selected because it would lead to easier and less expensive manufacturing. The blank width of 124 mm with a cylindrical punch (radius of 12.7 mm) was found to exhibit stable plane-strain state at the predicted failure site. Figures 6 and 7 include the temporal distribution of the strains and the ratio of the major to the minor strain, respectively. Figure 6 shows that the minor strain is very small throughout the monitored region. In Fig. 7 note that all the ratios of major to minor strain are greater than 7 along the entire centerline (in the stretching direction) of the blank.

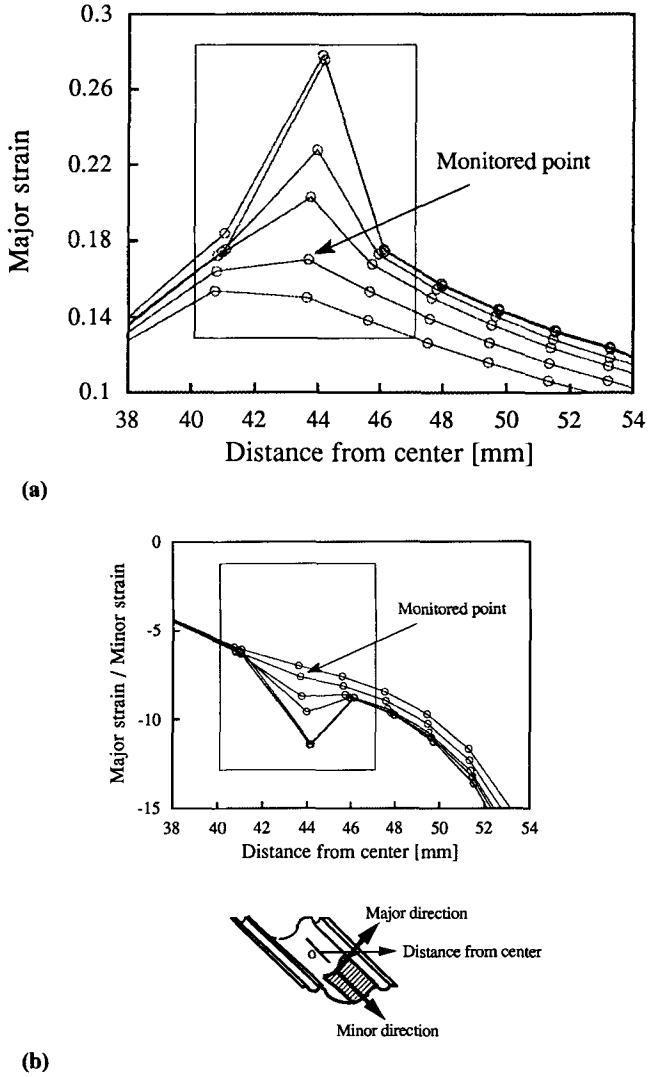

Fig. 3 (a) Typical temporal variation of major strain just before and after localization. To measure the plane-strain condition, the peak major strain just before the localization was picked up and divided by the corresponding minor strain. (b) Typical temporal variation of ratio of major to minor strain

4.2 *Phase II: Examination of Bending with ABAQUS*

Because the total geometry was reduced to a compact size, the bending influence by the smaller punch and die would become greater. Using ABAQUS, the strain pattern was observed in order to design the tool to generate the failure position as far as possible from the die side to avoid bending-dominant failure. Figure 8 illustrates the major strain distributions for different thicknesses of the blank at the punch height of 12.5 mm. The friction coefficient used in the computation was 0.15, same value used with the SHEET-3 calculation. Because minor strains with all thicknesses were very small, the magnitude and the position of peak thickness strains were almost the same as those of major strains. It was predicted that the failure would

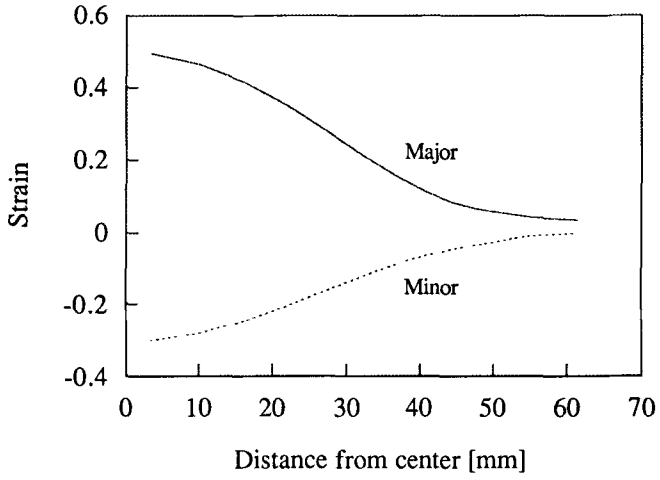

Fig. 4 Strain distributions for the same punch size (flat-elliptical) as that proposed originally with the blank approximately 1.4 times wider

take place in the die side when the thickness of the blank was increased to 1.5 mm. This failure mode is attributed to a bending influence because of tight radius of the die, which is undesirable. For lighter gages, the strain localization occurred at the punch side mainly by stretching. In this case, the failure position will move slightly either to the center of the punch or to the unsupported region toward the die side, depending on the lubrication condition. The predicted failure regions for lighter gages show blunt curves around the peak strain. This may indicate that the accurate simulation of the strain localization, which is not of present concern, requires more meshes. Actual evaluation of the peak strain can be extrapolated from the curve.

To cover heavier gage ranges up to approximately 1.5 mm with one set of the optimized tooling, the die radius was increased to 9.5 mm, which is approximately six times larger than the blank thickness of 1.5 mm. Employing this geometry, the ratio of major to minor strain near the predicted failure site just before the onset of strain localization reduced to approximately 5 from 7, according to the SHEET-3 calculation. Figure 9 shows the major strain distributions of the blank (thickness = 1.5 mm) with the larger die radius at different punch heights. The localization of the major strain took place at the punch side and the bending at the die did not affect the failure any more.

Based on this geometry, further tests were focused on examining the influence of lubrication and thickness of the blank to the failure mode because the lubrication condition also was predicted to affect the failure position as previously mentioned. Figure 10 shows the punch force versus punch height for different gages with $\mu = 0.25$, computed with both SHEET-3 and ABAQUS. This kind of diagram is useful for determining the punch-height-to-failure (PH_0) in the actual test, in which case the detection of the onset of strain localization is very difficult. In an LDH test, the LDH_0 (punch-height-to-failure in LDH test) is also determined by the punch force versus punch height curve recorded in the computer. As the punch moves up (or down), the punch force required to form the blank increases until the onset of failure, when the punch force starts to drop. Therefore, for practical purposes, the punch height at the peak

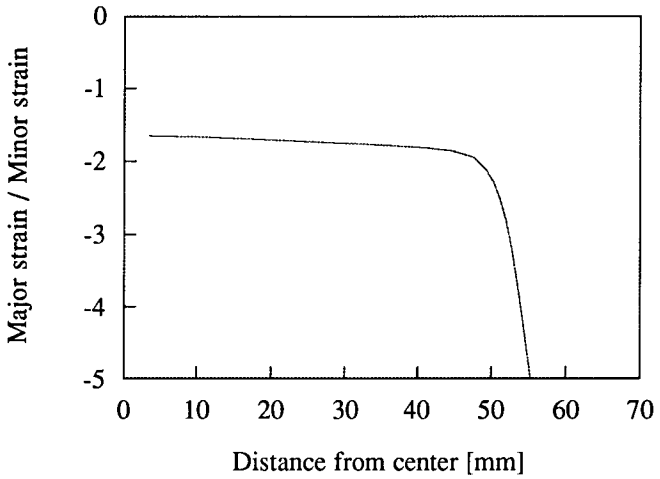

Fig. 5 Distribution of the ratio of major to minor strain for the same punch size (flat-elliptical) as that proposed originally with the blank approximately 1.4 times wider

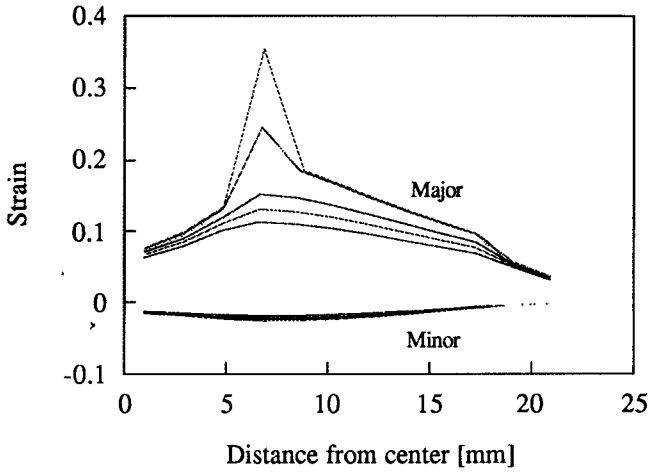

Fig. 6 Major and minor strain distributions for the reduced punch size (radius = 12.7 mm) with blank width of 124 mm

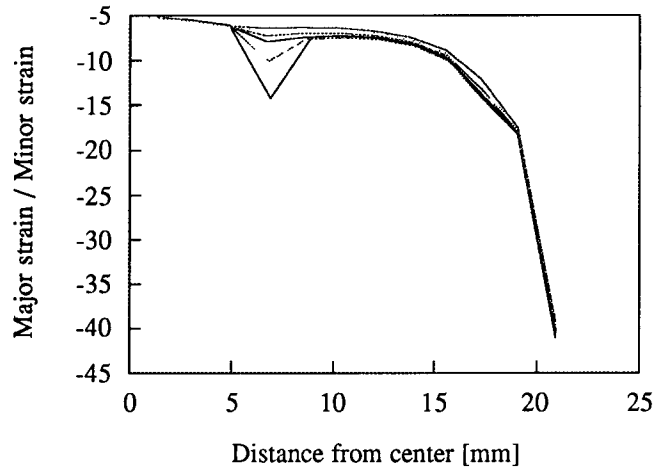

Fig. 7 Ratio of the major and the minor strain distributions for the reduced punch size (radius = 12.7 mm) with blank width of 124 mm

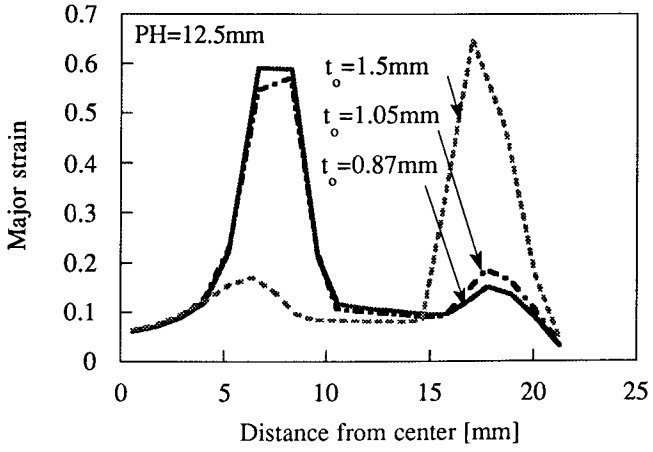

Fig. 8 Major strain distributions from ABAQUS for the compact size (radius = 12.7 mm) with the blank width of 124 mm. Data shown here are for different thicknesses of the blank at punch height of 12.5 mm. t_0 indicates the original thickness of the blank.

punch force can be interpreted as the punch-height-to-failure. In Fig. 10, the deviation of curves from SHEET-3 and ABAQUS became greater with the increase of the blank thickness. All the results from SHEET-3 share same PH_0 because they are independent of bending influence for different thicknesses. Meanwhile, the results from ABAQUS showed increasing PH_0 as the thickness increased up to t_0 = 2.0 mm. At t_0 = 2.4 mm, the PH_0 is the same as at t_0 = 2.0 mm. This was examined by plotting strain distributions. Figure 11 shows the distribution of major strain for different gages computed from ABAQUS when the peak major strain became greater than 0.5. All the blanks that have thicknesses up to 2.0 mm would fail near punch side, while the blank with t_0 = 2.4 mm would fail near the die side because the bending became more dominant

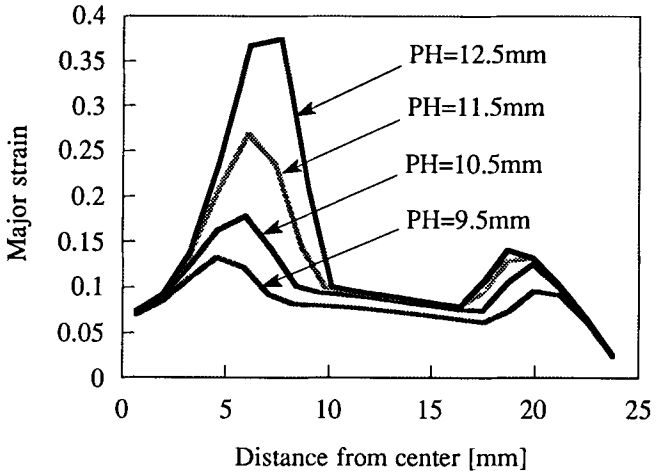

Fig. 9 Major strain distributions from ABAQUS for the compact size (radius = 12.7 mm) with blank width of 124 mm at different punch heights (*PH*). The radius of the die is 9.5 mm.

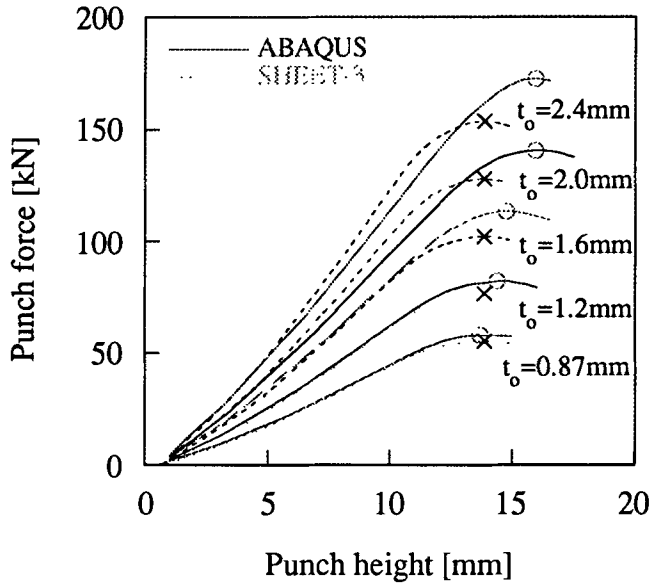

Fig. 10 Punch force versus punch height for different gages with μ = 0.25 from both SHEET-3 and ABAQUS. t_0 indicates undeformed blank thickness. "O" and "X" denote the peak punch force for ABAQUS and SHEET-3, respectively.

there. From this, the blank with t_0 = 2.4 mm was predicted to fail earlier at the die side before it was fully stretched at the punch side. The punch-height-to-failure, therefore, could not be increase as it could when stretching was dominant. Based on these findings, three different friction coefficients were considered in the computation to investigate the influence of lubrication on the failure mode for the final punch and the blank configurations. The results are shown in Table 1. In Table 1, for all the thickness ranges for well-lubricated condition (μ = 0.15), the blank would fail near the punch side. The higher μ and heavier gages contributed to the predicted failure taking place near the die side. From this table, it is suggested that the final geometry should be used with the blank thickness no greater than 1.5 mm to afford wide ranges of lubricating condition. This thickness limit is still much greater than the usual range of blank thicknesses used in automobile body panels (0.8 to 1.1 mm), for which the plane-strain failure is most seriously considered.

From the results obtained with SHEET-3 and ABAQUS, the final tool and blank geometries were determined and are shown in Fig. 12. The peak punch force predicted from this tooling for the blank of 1.5 mm thickness was less than 100 kN when μ = 0.25.

Table 1 Failure positions for different lubrication conditions and blank gauges

	Thickness, mm					
μ	0.866	1.2-1.5	1.6	2.0	2.4	3.0
0.15	P	P	P	P	P	P
0.25	P	P	P	P	D	D
0.35	P	P	D	D	D	D

Note: P: failure predicted to take place at the *punch* side; D: failure predicted to take place at the *die* side.

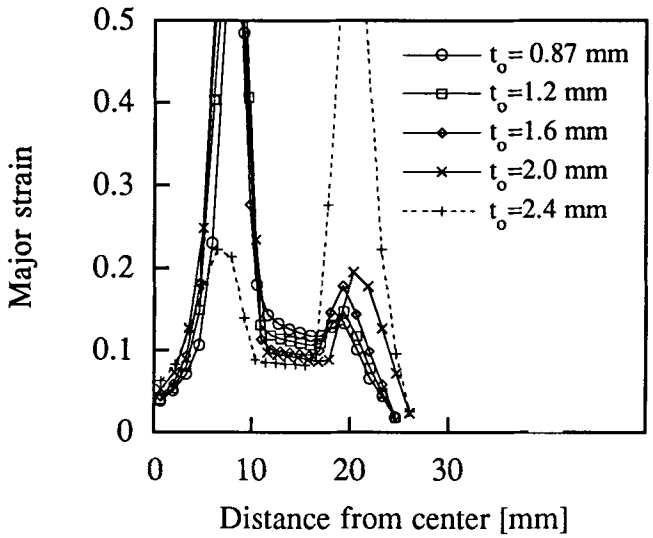

Fig. 11 Distribution of major strain for different gages with μ = 0.25 when the peak major strain became greater than 0.5 from ABAQUS. t_0 indicates undeformed blank thickness.

4.3 *Phase III: Simple Numerical Verifications*

To examine the performance of the optimized tooling, two types of tests were carried out—comparison with LDH test and a sensitivity analysis of OSUFT—using ABAQUS and SHEET-3, respectively.

4.3.1 Comparison with LDH Test

A standard LDH test, specified by the North American Deep Drawing Research Group (NADDRG), involves a procedure for finding the optimal blank width that promotes the best plane-strain state near the failure region. This requires several pretests by varying blank widths, generally from 114 to 140 mm, in increments that do not exceed 3 mm. In actual practice, the LDH test is performed for quality control (QC), in which case the procedure is shortened so that for most low-carbon, drawing-quality steels, a standard blank width of 133.4 mm (5.25 in.) is used. In this work, for a simple verification, the QC-type test was simulated. Material anisotropy was not considered. Values of $\mu = 0.25$ and $t_0 = 0.87$ mm were used for simulation. Figure 13 includes the schematic of both tests with undeformed and deformed meshes. Simulated results for both tests showed that the failure (in terms of large magnitude of the thickness strain) would initiate on the punch side and near the symmetry axis in the stretching direction. The failure then would propagate toward transverse and radial directions for the OSUFT and the LDH test, respectively. The area of plane-strain region was observed based on this information, when the thickness strains became greater than 0.6. Figure 14 includes the directions of interest for both tests. The dark circle denotes a position of the peak thickness strain, where the onset of the failure was predicted. X and Y are global coordinates that indicate

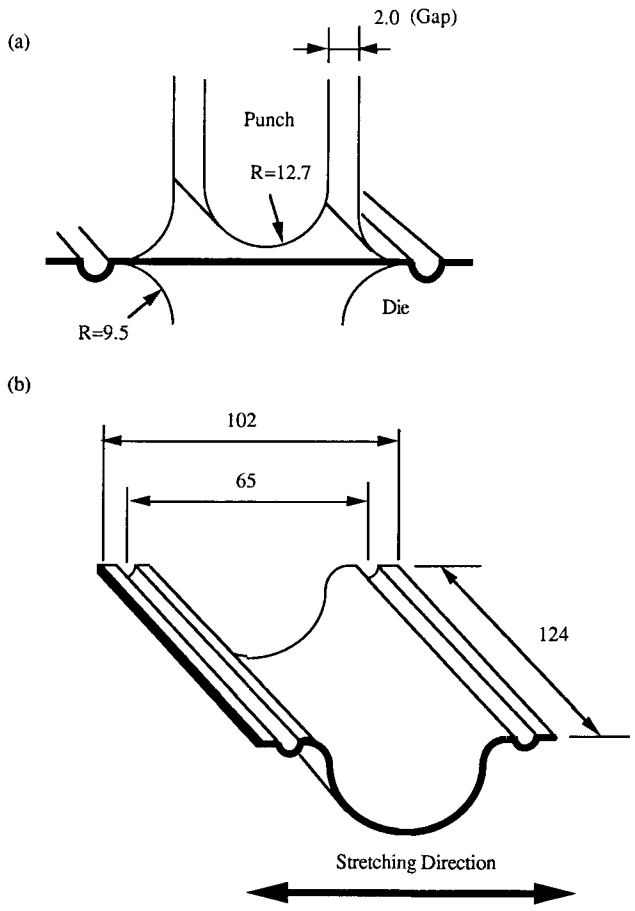

Fig. 12 (a) Schematic of the optimized tool geometry and (b) the deformed blank with important dimensions. (Dimension shown here does not change with the deformation.) Units are given in mm.

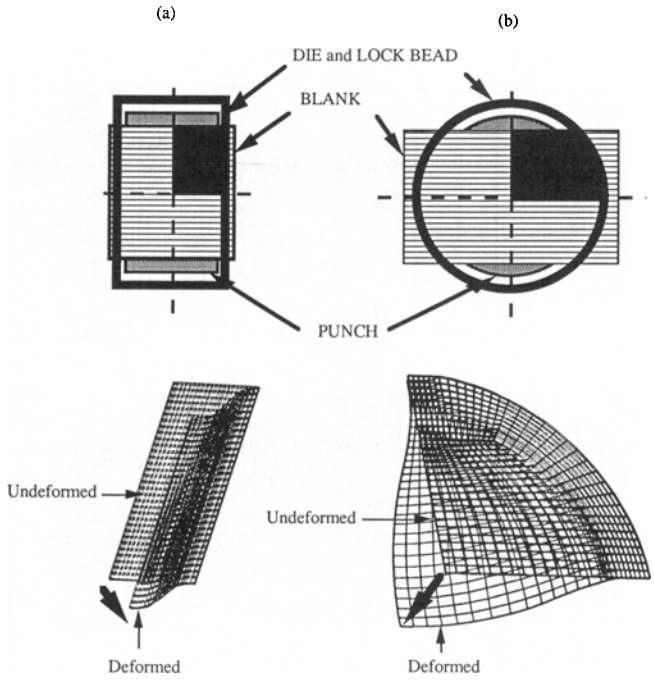

Fig. 13 Schematic (top view) and finite-element meshes (below) of (a) the OSUFT and (b) the LDH test. Because of symmetry, only the regions displayed with black were modeled. Bold arrows indicate the punch direction.

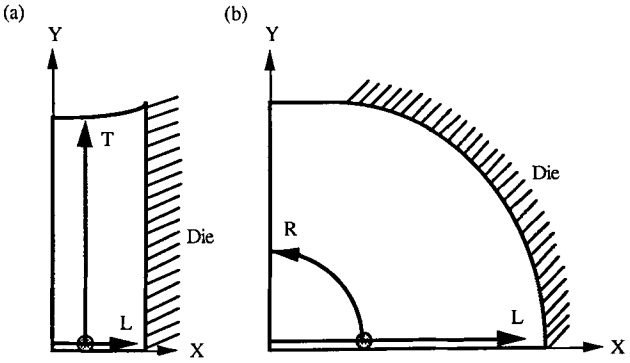

Fig. 14 Direction of interest for (a) the OSUFT and (b) the LDH test. The dark circle denotes a position of the peak thickness strain, where the initiation of the failure was predicted. X and Y are global coordinates that indicate stretching direction and the one perpendicular to it. L, T, and R indicate longitudinal (stretching), transverse, and radial directions. Failures (in terms of large magnitude of thickness strain) were initiated at dark circles and propagated in the transverse and radial directions for the OSUFT and the LDH test, respectively.

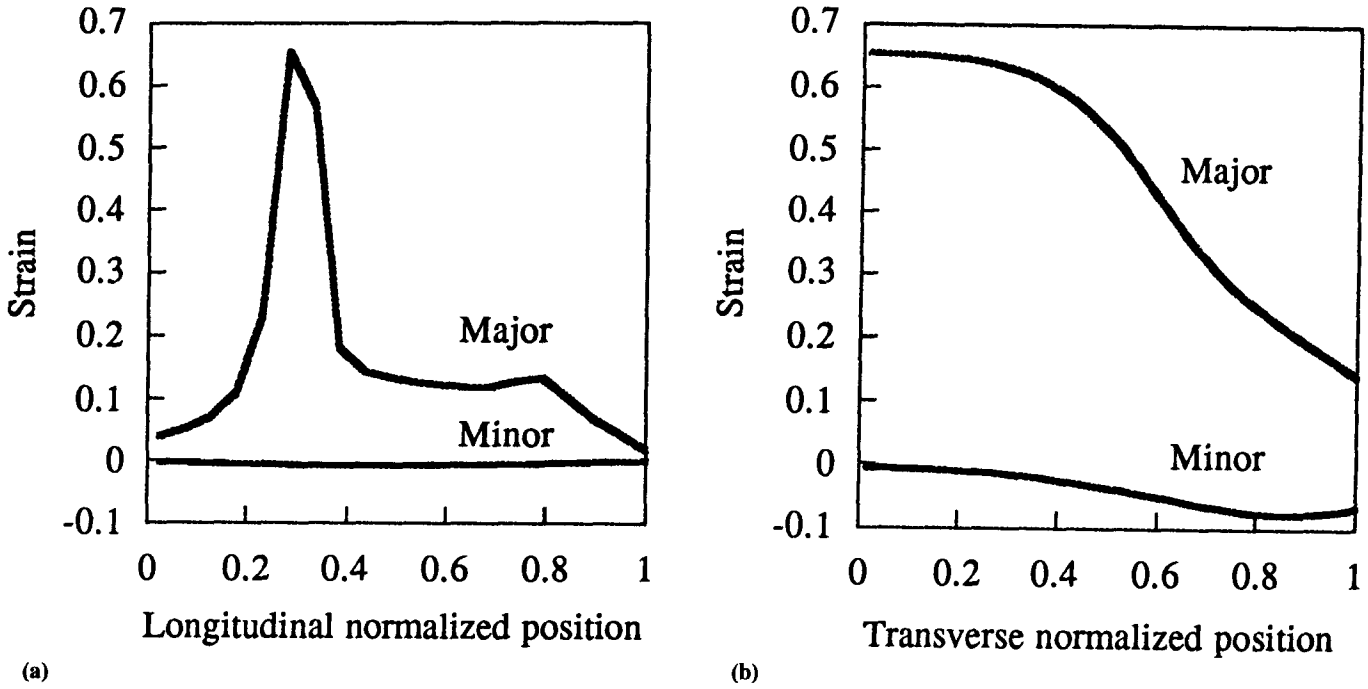

Fig. 15 Major and minor strain distributions of the OSUFT when the thickness strain became greater than 0.6. (a) Longitudinal direction. (b) Transverse direction. The position was normalized by dividing the original blank width.

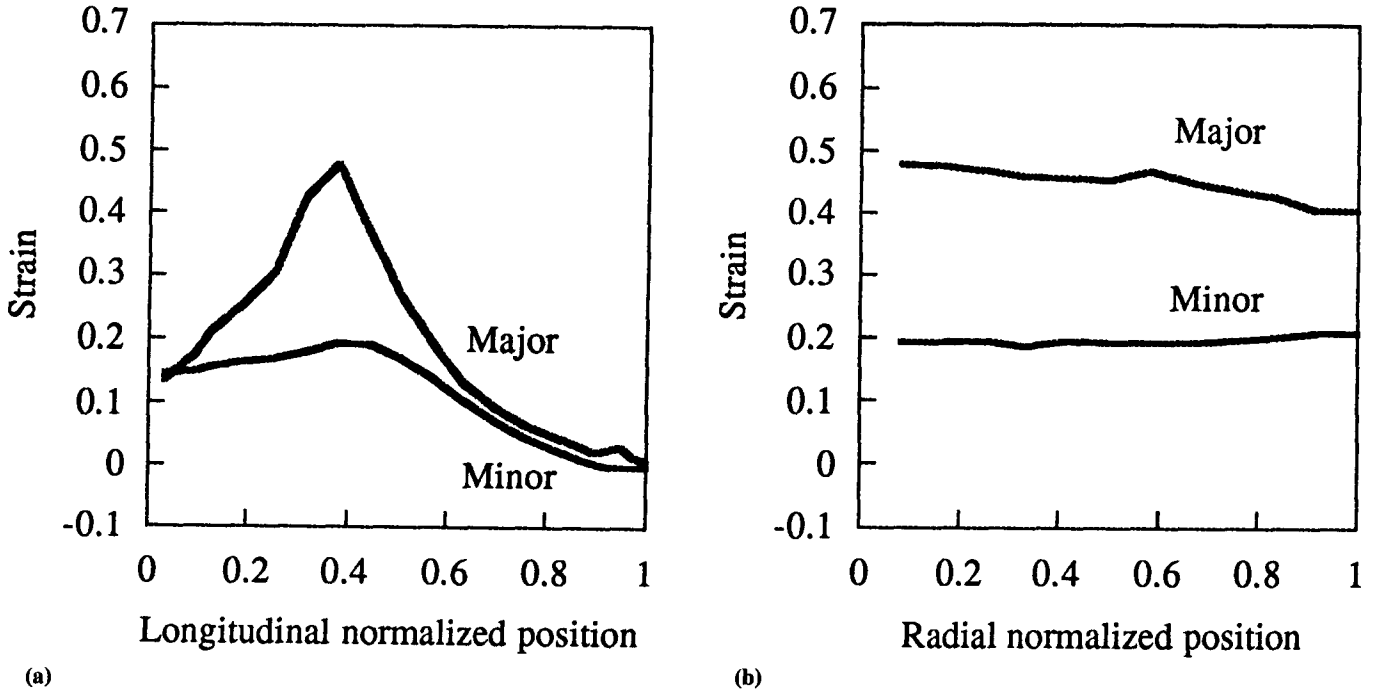

Fig. 16 Major and minor strain distributions of the LDH test when the thickness strain became greater than 0.6. (a) Longitudinal direction. (b) Radial direction. The position was normalized by dividing the circular arc length as shown in Fig. 14.

stretching direction and the one perpendicular to it, respectively. L, T, and R indicate longitudinal (stretching), transverse, and radial directions, respectively. Figure 15 shows major and minor strain distributions of the OSUFT when the thickness strain became greater than 0.6. The position was normalized by dividing the original blank width. Therefore 0 indicates the position at the symmetry axis in the stretching direction and 1 indicates the position at the free lateral surface of the blank. Both in the longitudinal (stretching) and transverse directions, the minor strain was very small and the plane-strain area was pre-

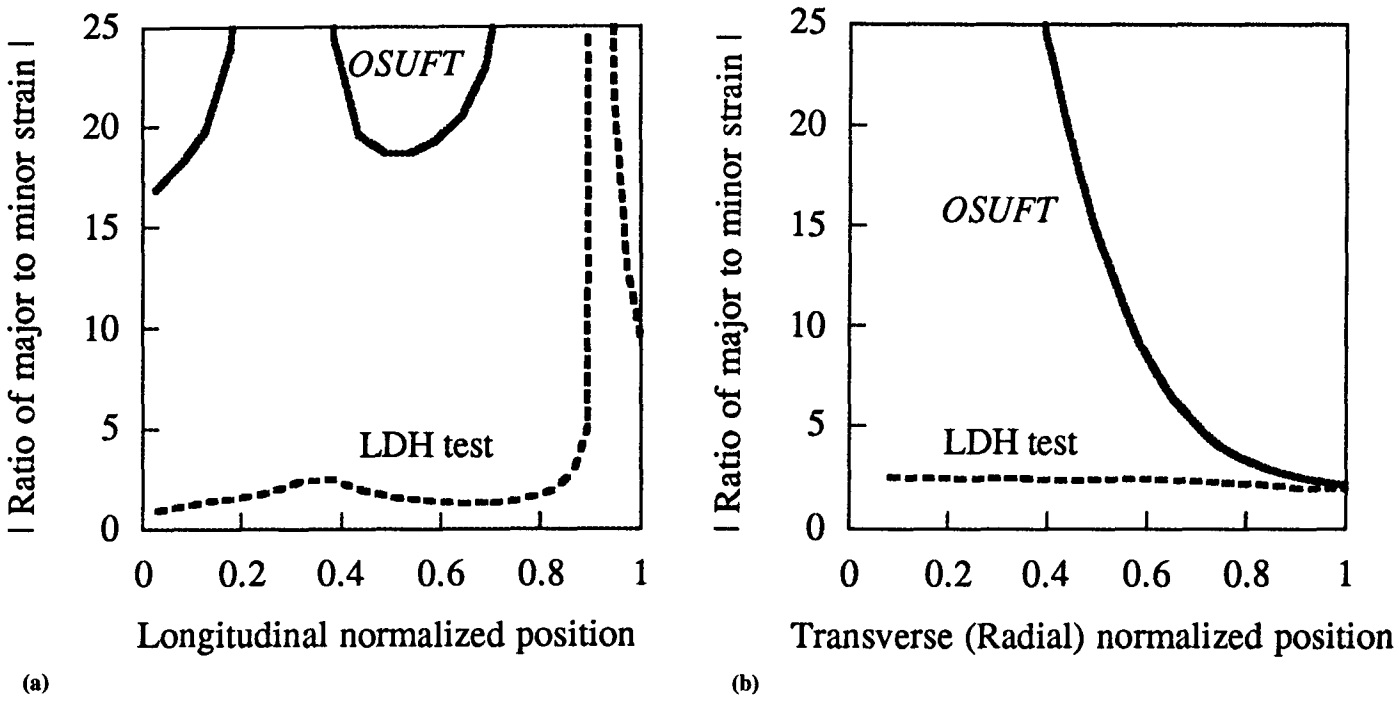

Fig. 17 Ratio of major to minor strain from the simulation of both tests. (a) Longitudinal (stretching) direction. (b) Transverse (or radial) direction

dicted to be larger in comparison with Fig. 16 where same type of plots for the LDH test are shown. In the LDH test, the minor strain near the predicted failure region is very large (~0.2) and plane strain is not likely to occur. To observe the plane-strain state better, a quantitative comparison was made such that the ratio of major to minor strain was plotted for same positions (see Fig. 17). Because the minor strains of the two tests have opposite signs, the absolute numbers were compared. Figure 17(a) shows the ratio in the longitudinal direction. The least ratio of the OSUFT was greater than 16, which indicates that the entire axis represents plane strain very well. However, with the LDH test, the ratio near the predicted failure site is not greater than 3, which shows that the plane strain is not likely to occur. Even in the transverse direction, the OSUFT has a fairly large region of plane strain (5 times larger major strain than minor strain up to the normalized position of 0.7). For LDH, the ratio in the radial direction is about 2.5 and plane strain is not well represented. Figure 18 displays the strain paths of both tests from the undeformed state to the deformed state when the thickness strain became greater than 0.6. The path was monitored at the element that eventually showed peak thickness strain. The OSUFT showed a more proportional strain path than did the LDH test, maintaining very small minor strains. The proportionality of the strain path contributes to less susceptibility to variations in process parameters, such as surface conditions, and to a more effective correlation with press performance. In summary, the enhanced OSUFT was predicted to represent much better plane-strain state and larger plane-strain area near the predicted failure site than would the QC-type LDH test. It was also predicted to have a more proportional strain path during the test, which enhances the repeatability of the test.

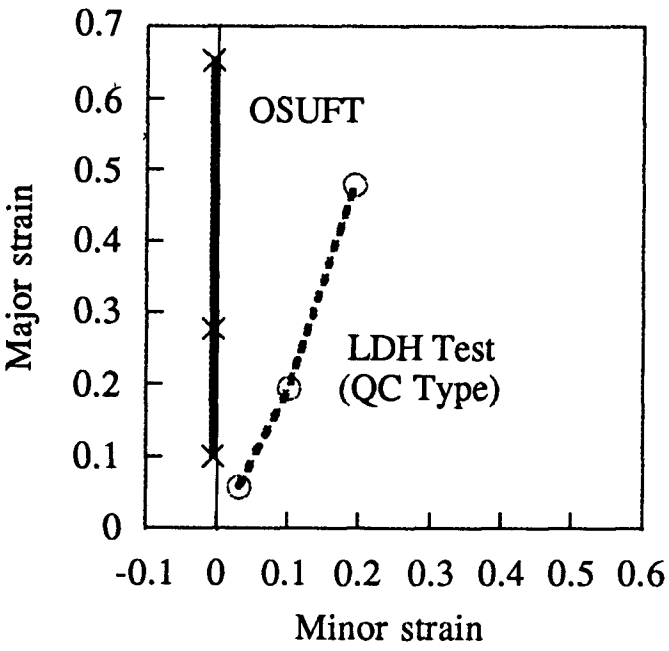

Fig. 18 Strain paths of both tests from the undeformed state to the deformed state when the thickness strain became greater than 0.6

4.3.2 Sensitivity Analysis

Another brief performance test was carried out by examining the sensitivity of the punch-height-to-failure (PH_0) on the strain-hardening exponent (n), the normal anisotropy (r), and the friction coefficient (μ). The punch-height-to-failure is very

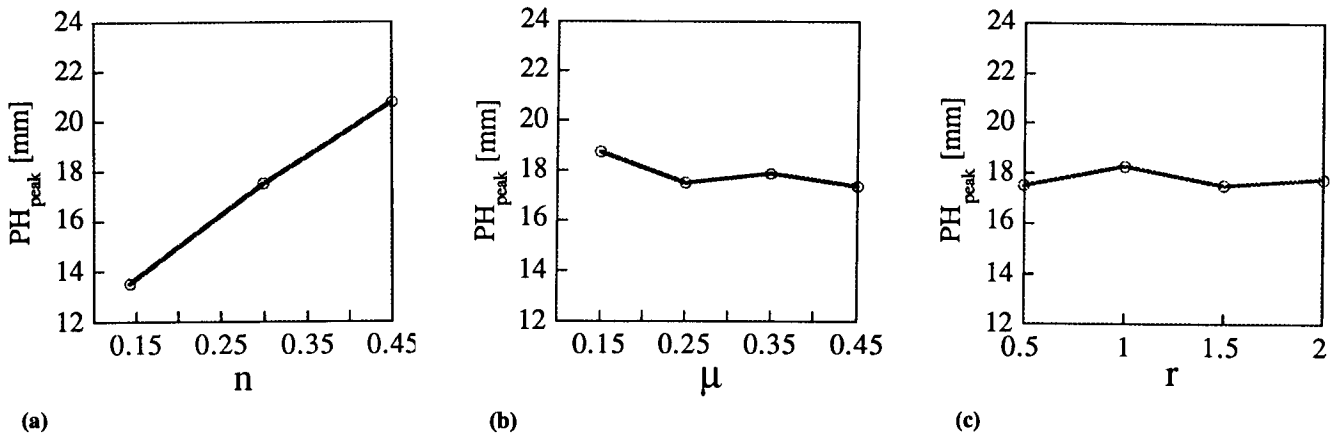

Fig. 19 Sensitivity of the punch-height-to-failure (*PH*) on (a) the strain-hardening exponent (n), (b) the friction coefficient (μ), and (c) the normal anisotropy (r)

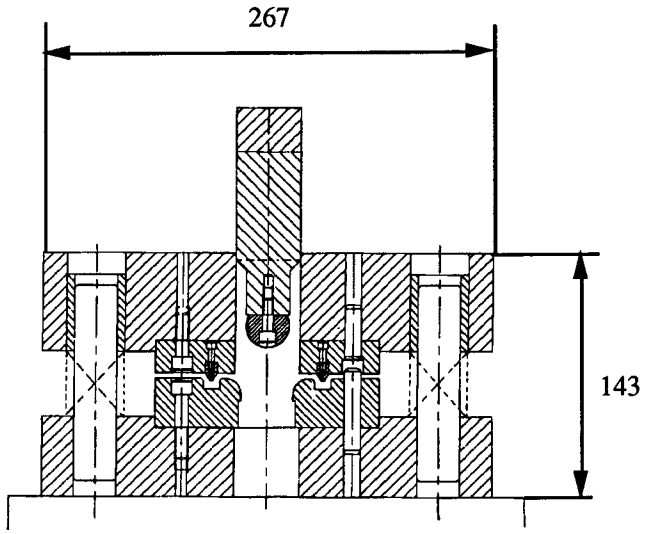

Fig. 20 Front view of the modular system with the optimized tool (closed position). The outside dimensions are specified in mm.

useful in practical testing to correlate with the press performance. If the PH_0 is too sensitive on the lubrication state and material anisotropy, poor repeatability from test to test is expected. Using SHEET-3, the PH_0 was obtained from the peak of the punch force/punch height curve for different parameters. Figure 19 shows the computed results. As n increases, the PH_0 increases almost proportionally. With varying lubrication states, although the PH_0 decreases with increasing μ, the variation of *PH* is very small. With different normal anisotropy, the PH_0 does not change much either. Therefore, it is expected that the enhanced geometry would show little sensitivity (in terms of the punch-height-to-failure) on the lubrication states and materials anisotropy, which again will contribute to the better repeatability of the test.

4.3 *Phase IV: Manufacture of the Prototype System*

Based on the optimized geometry determined by the computer simulation, the prototype of the tooling was designed and manufactured. Figure 20 shows the front view of the modular system with the optimized tool. This tooling was designed to be used with any kind of press with an appropriate adapter for the punch stem, which is inexpensive to make. Initial tests with the prototype system showed that the failure site for several materials (AK-steel, high-strength galvanized steel, and brass with initial thickness less than 1 mm) were very consistent such that all the positions lied on the unsupported region near the punch side. All the failures were initiated from the symmetry axis (along the stretching direction) of the blanks, where the plane strain is most likely. Experimental comparisons of the three tests were made and the standard deviation of the failure punch height with 70/30 brass, high-strength galvanized (HSG) steel, IF steel, and Univit steel sheets is displayed in Fig. 21. As shown, the optimized test reduced scatter by nearly an order of magnitude with respect to the LDH test.

5. Summary and Conclusions

Using three-dimensional finite-element method, the test configuration of the O.S.U. Formability Test was enhanced by making its size as compact as possible and yet able to produce consistent plane-strain failure for different materials and processing conditions. SHEET-3 was used to find the optimal geometry considering anisotropy, while ABAQUS was used to examine the bending effect. By simulative trial and error, a compact tool geometry was found that generated stable plane strain up to failure such that the ratio of the major to minor strain at the onset of the failure was greater than 5. This geometry was designed to have low punch force and to avoid bending failure for materials with r-values up to 2.0, friction coefficient ranges of 0.15 to 0.35, and thicknesses up to 1.5 mm. Simulative comparison with the LDH test showed that the enhanced test configuration will provide larger plane-strain area near the predicted failure region on the blank and produce a more proportional strain path. Further FEM calculations predicted that actual test results will be extremely insensitive to the lubrication state and material anisotropy, which will contribute to better repeatability of the test. The test with prototype tooling showed very consistent failure mode and location with several

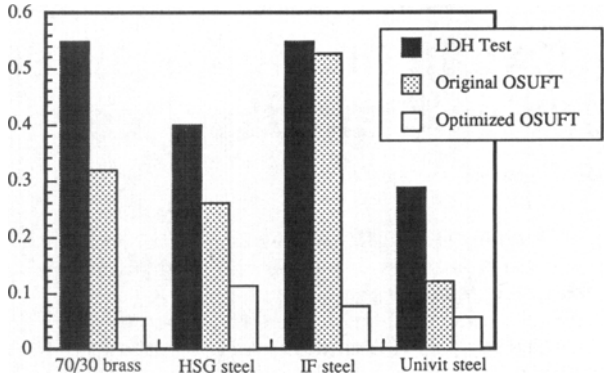

Fig. 21 Comparison of the scatter from different test geometries. The standard deviation of the punch-height-to-failure is directly related to the scatter of the measurement.

materials. Experiments revealed that the optimized tool showed significantly less scatter in measurement compared with that of the LDH and the original O.S.U. Formability tests.

Acknowledgments

This research was sponsored by the Edison Materials Technology Center (EMTEC) of Kettering, OH, under project No. CT-28. The use of the CRAY Y-MP8/864 was made possible through a grant, PAS080, from the Ohio Supercomputer Center, Columbus, OH. R.J. Davis of the First Tool Corporation provided a partial donation in manufacturing the prototype modular system. The first author (Y.S.S.) would like to acknowledge F.I. Saunders, W. Wang, and D. Zhou for many helpful discussions on this work and S. Sadagopan who contributed to an innovative design of the prototype modular system based on the optimized geometry.

References

1. A.S. Kasper, How We Will Predict Sheet Metal Formability, *Met. Prog.*, Oct 1969, p 159-160
2. J. Gronostjski and C. Banasiak, The Effect of Anisotropic Plasticity and Work-Hardening on the Sheet Metal Drawability, *Sheet Metal Forming and Energy Conservation,* Ninth Biennial Congress, International Deep Drawing Research Group, American Society for Metals, 1976, p 81-96
3. S.S. Hecker, A Cup Test for Assessing Stretchability, *Met. Eng. Q.*, Vol 14, 1974, p 30-36
4. A.K. Ghosh, The Effect of Lateral Drawing-In on Stretch Formability, *Met. Eng. Q.*, Vol 15, 1975, p 53-64
5. R.A. Ayres, W.G. Brazier, and V.F. Sajewski, Evaluating the GMR-Limiting Dome Height Test as a New Measure of Press Formability Near Plane Strain, *J. Appl. Met. Work.*, Vol 1, 1979, p 41-49
6. D.J. Meuleman, J.L. Siles, and J.J. Zoldak, "The Limiting Dome Height Test for Assessing the Formability of Sheet Steel," Technical Paper Series 850005, SAE International Congress & Exposition (Detroit), 25 Feb to 1 March 1985, Society of Automotive Engineers
7. A.F. Graf and N. Izworski, "Industrial Implementation of Practices for LDH Stability," Technical Paper Series 930816, Sheet Metal and Stamping Symposium SP-944, Society of Automotive Engineers, 1993, p 303-307
8. M.P. Miles, "A Better Sheet Formability Test," M.S. Thesis, Ohio State University, 1991
9. M.P. Miles, J. Siles, R.H. Wagoner, and K. Narasimhan, A Better Sheet Formability Test, *Metall. Trans. A,* Vol 24A, 1993, p 1143-1151
10. Y. Germain, K. Chung, and R.H. Wagoner, A Rigid-Viscoplastic Finite Element Program for Sheet Metal Forming Analysis, *Int. J. Mech. Sci.,* Vol 31, 1989, p 1-24
11. Y.T. Keum, E. Nakamachi, R.H. Wagoner, and J.K. Lee, Compatible Description of Tool Surfaces and FEM Meshes for Analysing Sheet Forming Operations, *Int. J. Num. Meth. Eng.,* Vol 30, 1990, p 1471-1502
12. R.H. Wagoner and D. Zhou, Analyzing Sheet Forming Operation—Recent Numerical and Experimental Advances, *Numerical Methods in Industrial Forming Processes—NUMIFORM 92,* J.L. Chenot, R.D. Wood, and O.C. Zienkiewicz, Ed., A.A. Balkema, Rotterdam, Netherlands, 1992, p 123-132
13. ABAQUS v.4.9 at the Ohio Supercomputer Center, under academic license from Hibbitt, Karlsson & Sorensen, Inc., Pawtucket, RI, 1991
14. R. Hill, Theoretical Plasticity of Textured Aggregates, *Math. Proc. Camb. Phil. Soc.,* Vol 85, 1979, p 179-191
15. R. Hill, A Theory of the Yielding and Plastic Flow of Anisotropic Metals, *Proc. R. Soc. London,* Vol 193A, 1948, p 281-297
16. F.I. Saunders and R.H. Wagoner, Finite Element Modeling of a New Sheet Formability Test, *Computer Applications in Shaping and Forming of Materials,* M.Y. Demery, Ed., TMS, 1993, p 205-220
17. T.B. Stoughton, Finite Element Modeling of 1008 AK Sheet Steel Stretched over a Rectangular Punch with Bending Effects, *Computer Modeling of Sheet Metal Forming Process: Theory Verification and Application,* N.M. Wang and S.C. Tang, Ed., TMS-AIME, 1985, p 143-159
18. J.A. Schey, *Tribology in Metalworking,* American Society for Metals, 1983
19. R.H. Wagoner, Measurement and Analysis of Plane Strain Work Hardening, *Metall. Trans. A,* Vol 11A, 1980, p 165-175
20. Forming and Forging, *Metals Handbook,* ASM International, 1988
21. M.P. Miles, K. Narasimhan, F.I. Saunders, Y.S. Suh, R.H. Wagoner, and J. Siles, "A Better Test to Evaluate Sheet Formability," EMTEC/CT28/TR-92-28, Edison Materials Technology Center, 1992